Available online at www.sciencedirect.com
SCIENCE DIRECT
Journal of Solid State Chemistry 179 (2006) 1445–1452
JOURNAL OF SOLID STATE CHEMISTRY
www.elsevier.com/locate/jssc

Improvement of Er^{3+} emissions in oxyfluoride glass ceramic nano-composite by thermal treatment

Daqin Chen, Yuansheng Wang*, Yunlong Yu, En Ma

The State Key Laboratory of Structural Chemistry, Fujian Institute of Research on the Structure of Matter, Chinese Academy of Sciences, Fuzhou, Fujian 350002, China

Received 11 December 2005; received in revised form 25 January 2006; accepted 28 January 2006
Available online 28 February 2006

Abstract

In order to improve the 1.53 μm emission of Er^{3+}-doped oxyfluoride glass ceramic containing CaF_2 nano-crystals, series of samples with same Er^{3+} doping lever thermal treated under different conditions were prepared. The UV-VIR-NIR absorption spectra, near-infrared and up-conversion emission spectra, and $^4I_{13/2}$ decay curves were measured. Based on Judd–Ofelt theory, the radiative transition probability, fluorescence branching ratio and radiative decay time of various metastable transitions of precursor glass and glass ceramics were evaluated. With the increasing of heating temperature, the Judd–Ofelt intensity parameter Ω_2 monotonously decreased from 4.39×10^{-20} to 2.72×10^{-20} cm^2; the emission lifetime and quantum efficiency significantly increased from 5.9 to 8.0 ms and 70% to 98%, respectively. The wavelength dependence of gain cross-sections of oxyfluoride glass and glass ceramics were computed to be relatively flat in the range of 1530–1565 nm for population inversion from 0.7 to 1.0.

Keywords: Oxyfluoride glass ceramics; CaF_2 nano-crystals; Judd–Ofelt theory; Luminescence

1. Introduction

With the success of the erbium-doped fiber amplifiers (EDFA), it is well known that the fluoride environment is preferred over the oxide one mainly to avoid non-radiative transitions [1]. The solubility of the rare earth is also larger in the fluoride medium than in the oxide [2]. Among fluorides, CaF_2 is a promising candidate of desired host materials for its high solubility of both sensitizer and activator rare-earth ions and highly transparent from 0.13 to 9.5 μm [3]. However, the synthesis of fluoride crystals is complicated, and the stability and fiberizability as pratical materials still remain problematic. Thus, a good solution would be Er^{3+}-doped oxyfluoride glass ceramic composite, i.e., fluoride crystallites embedded among an oxide glassy matrix with high chemical and mechanical stabilities [4–7]. In order to enhance the luminescence properties of oxyfluoride glass ceramics, the partition of rare-earth ions into fluoride crystalline environment with large band gap and low phonon energy is necessary [4].

Judd–Ofelt theory [8,9] is very useful in estimating the probability of the forced electric dipole transitions of rare-earth ions in various environments. Using this theory, three intensity parameters could be deduced from the measured absorption spectra of host materials, which could be further used to evaluate the optical performance, such as the radiative transition probability, the oscillator strength, the branching ration, and the spontaneous emission probability. Based on Judd–Ofelt theory, spectroscopic properties of rare-earth ions in several oxyfluoride glasses and glass ceramics have been studied [10–18]. Since it is very difficult to partition all the rare-earth ions into the precipitated fluoride crystallites, the obtained spectroscopic parameters are considered to originate from rare-earth ions in both fluoride crystals and glassy matrix [14]. In our previous work [14], the effect of Er^{3+} content on spectroscopic properties of oxyfluoride glass ceramics containing CaF_2 nano-crystals was systematically investigated. It is well known that, besides the content of Er^{3+}, the thermal treatment condition, which determines the microstructure

*Corresponding author. Fax: +86 591 8370 5402.
E-mail address: yswang@fjirsm.ac.cn (Y. Wang).

0022-4596/$ - see front matter © 2006 Elsevier Inc. All rights reserved.
doi:10.1016/j.jssc.2006.01.056

of glass ceramic, may also greatly affect the luminescence of the material. In this paper, series of oxyfluoride glass ceramics containing CaF_2 nano-crystals doped with a fixed content of Er^{3+} thermal treated at various conditions were studied in order to improve Er^{3+} emissions. Based on the quantitative analysis of absorption, emission spectra and luminescence lifetimes, the suitability of this host material as a candidate for 1530 nm amplifier was evaluated.

2. Experimental details

The precursor glass doped with 2.4×10^{20} ions/cm^3 Er^{3+} was prepared with the following composition (in mol%): $44.5SiO_2$–$24.8Al_2O_3$–5.0CaO–9.9NaF–$14.8CaF_2$ (donated as sample G). The doping of Er^{3+} was achieved by adding suitable amount of ErF_3. For each batch, about 20 g of starting materials of high purity (>3 N) were fully mixed and melted in a covered platinum crucible in air atmosphere at 1350 °C for 1.5 h, and then cast into a brass mold followed by annealing at 450 °C to relinquish the inner stress. Er^{3+}-doped CaF_2 nano-crystals with different sizes among glassy matrix were obtained by heating precursor glass at 600, 630, 650 and 670 °C and hold 2 h, respectively (donated as sample 600, 630, 650, and 670 GC, respectively).

To identify the crystallization phase, XRD analysis was carried out with a powder diffractometer (DMAX2500 RIGAKU) using Cu$K\alpha$ radiation at 40 kV and 100 mA. A transmission electron microscope (TEM, JEM-2010) was used to investigate the microstructures of the samples. Sample densities were determined by the Archimedes' method using distilled water as medium. Refractive indices were measured by the prism minimum deviation method. To simplify the computation, the refractive index measured at a specific wavelength was used in spectroscopic analysis for the whole range of spectra. The absorption spectra in the range of 200–2000 nm were recorded on a spectrophotometer (Lambda900, Perkin-Elmer) with a resolution of 0.5 nm. The emission spectra were recorded under 980 nm excitation light from a 450 W Xenon lamp. Using an InP/InGaAs photomultiplier tubes (PMT), the infrared luminescence signals through the emission monochromator (M300) were detected. The fluorescence decay curves at 1530 nm were recorded with an NIR PMT (R5509) under the excitation of 980 nm by a microsecond flash lamp (900 μF). The visible up-conversion luminescence excited with a 30 mW diode laser at 980 nm was detected with a PMT detector (R928). All the above measurements were carried out at room temperature.

3. Results and discussion

3.1. Structural characterizations

The XRD patterns obtained from precursor glass and glass ceramics heat-treated at different temperatures are shown in Fig. 1. The precursor glass shows the amorphous humps, while after heating, several CaF_2 crystalline peaks appear in the diffraction curve. Based on the peak width and Debby–Scherrer formula, the mean sizes of CaF_2 crystals for glass ceramics heat-treated at different temperatures are evaluated to be about 5, 9, 15 and 38 nm, respectively. For 650GC sample, the TEM micrograph, as presented in Fig. 2(a), demonstrates the homogeneous distribution of spherical CaF_2 crystals with 12–18 nm in size among the glassy matrix, which might be a key factor determining the optical properties of glass ceramic [19]. The corresponding selected area electron diffraction (SAED) pattern, shown in Fig. 2(b), presents the polycrystalline diffraction rings of CaF_2 nano-crystals.

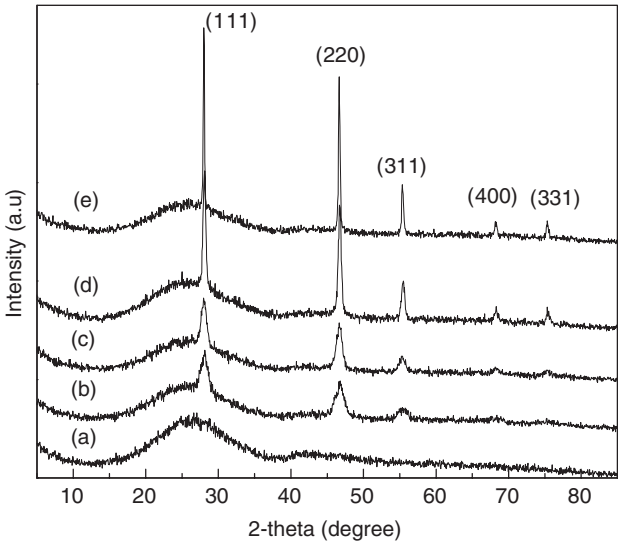

Fig. 1. XRD patterns of (a) precursor glass, and glass ceramics obtained by thermal treatment at (b) 600 °C, (c) 630 °C, (d) 650 °C and (e) 670 °C, respectively.

3.2. Absorption spectra and Judd–Ofelt analysis

The absorption spectrum of precursor glass in the range from 350 to 1650 nm is shown in Fig. 3. The absorption peaks, corresponding to the transitions from the ground state $^4I_{15/2}$ to the excited states, are marked in the figure. The UV absorption edge, which limits the transparency of sample at shorter wavelength, is caused by the electronic transitions of the host glass. Compared to that of the precursor glass, the obvious decrease of optical density for the transitions of $^4I_{15/2} \rightarrow {}^4G_{11/2}$ and $^4I_{15/2} \rightarrow {}^2H_{11/2}$ in glass ceramic, as shown in the inset of Fig. 3, implies that the circumstance or ligand field around Er^{3+} ions must have been altered, since these two transitions are sensitive to the environment around the active ions [20]. It is useful to analyze all these absorption transitions in terms of the standard Judd–Ofelt theory. It is well known that the transitions to $^4G_{11/2}$ and $^2H_{11/2}$ are determined by the intensity parameters Ω_2, Ω_4 and Ω_6, the transitions to $^4F_{9/2}$ and $^4F_{7/2}$ by Ω_4 and Ω_6, and the transitions to $^4F_{5/2}$ and $^4F_{3/2}$ by just one parameter Ω_6. As shown in the inset of

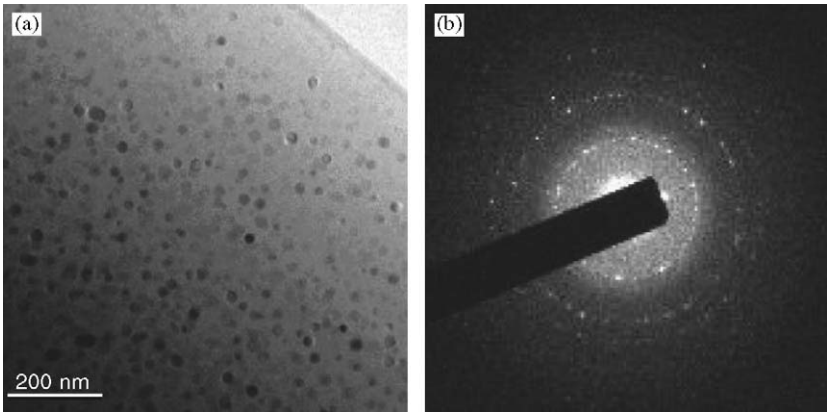

Fig. 2. TEM micrograph and the corresponding selected area electron diffraction (SAED) pattern of 650 GC sample.

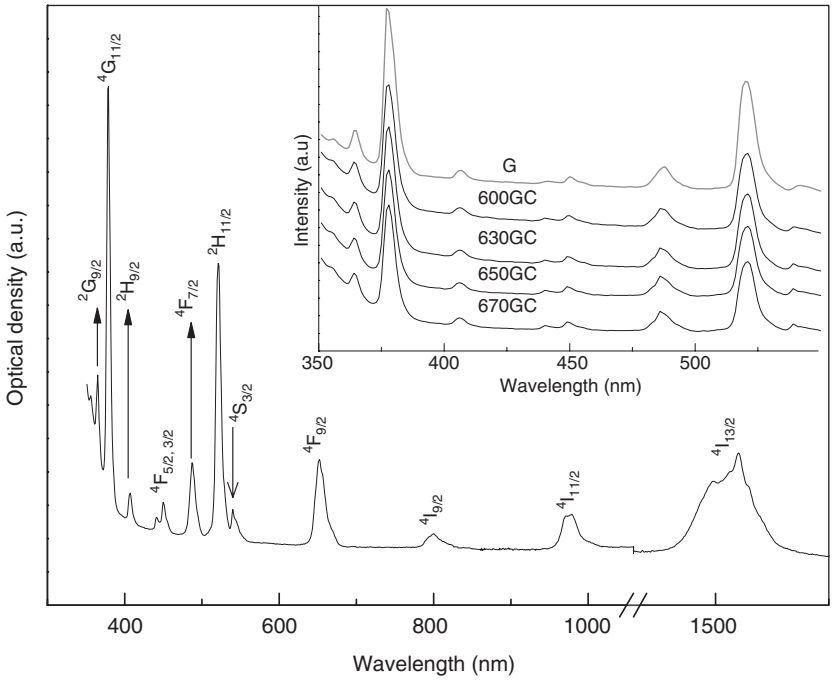

Fig. 3. Room temperature absorption spectrum of precursor glass; the inset shows the enlarged absorption spectra of precursor glass and glass ceramics in the range from 350 to 550 nm.

Fig. 3, the intensities of the $^4I_{15/2}\rightarrow{}^4G_{11/2}$ and $^4I_{15/2}\rightarrow{}^2H_{11/2}$ transitions are obviously changed with heating temperature, while those of the remaining ones keep almost the same. In the language of the theory, this behavior should be attributed to the variation of intensity parameter Ω_2. With the help of absorption spectra, experimental oscillator strengths for precursor glass and glass ceramics were obtained. These values were used to calculate the Judd–Ofelt intensity parameters $\Omega_{2,4,6}$ by a least-square program to yield the best fit with theoretical oscillator strengths. The variations of Judd–Ofelt intensity parameters versus thermal treatment temperatures are shown in Fig. 4. According to Judd–Ofelt theory, Ω_2 is sensitive to the environmental configuration symmetry of rare-earth ions, and it decreases with the host changing from oxides to fluorides [21–24]. On the other hand, Ω_6 increases usually with the covalence decreasing between rare-earth ions and the surrounding elements [25]. From precursor glass to glass ceramics, the value of Ω_2 greatly decreases. This may be explained as follows: with increasing of thermal treatment temperature, the crystallized fraction and the crystallinity of CaF_2 nano-crystals containing Er^{3+} increase, thus leading more Er^{3+} ions to locate at a more symmetrical site, which results in the decrease of Ω_2 [16]. However, the value of Ω_6 is almost unchanged within the error scope (about 5%), indicating the rigidity stability of the material [12]. It is worthy to note that the parameters for glass ceramics are originated from Er^{3+} ions in nano-crystals and residual ones in glass matrix.

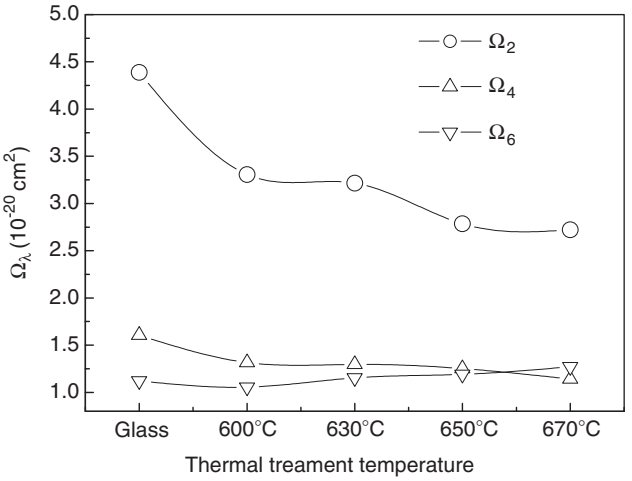

Fig. 4. Variation of Judd–Ofelt intensity parameters of glass ceramic obtained by different heating temperatures. The error of the least-square fit is about 5%.

The Judd–Ofelt intensity parameters can be used to calculated the radiative transition probability (A_{rad}) using the expression [26]

$$A_{\mathrm{rad}}[(S,L)J,(S',L')J'] = \frac{64\pi^4 e^2}{3h(2J+1)\lambda^3}\frac{n(n^2+2)^2}{9} \times \sum_{t=2,4,6}\Omega_t|<(S,L)J||U^{(t)}||(S',L')J'>|^2 + \frac{4\pi^2 e^2 hn^3}{3m^2c^2(2J+1)\lambda^3}|<(S,L)J||L+2S||(S',L')J'>|^2, \quad (1)$$

where J and J' are the total angular momentum quantum number of the initial and final states, respectively, $U^{(t)}$ ($t = 2, 4, 6$) unit tensor operators whose matrix elements had been calculated by Carnall et al. [26] and shown in Table 2, h the Planck constant, e the charge of electron, m the mass of electron, c the velocity of light, λ the wavelength, n the refractive index of samples and assumed to be same at different wavelength ($n = 1.520$) for precursor glass and glass ceramics.

The radiative lifetime of an emitting state is related to the total spontaneous emission probability of all the transitions from an excited state by

$$\tau_{\mathrm{rad}} = \left(\sum A_{JJ'}^{-1}\right). \quad (2)$$

The luminescence branching ratio of a transition is obtained from the expression

$$\beta_{J'J} = A_{JJ'}\tau_{\mathrm{rad}}. \quad (3)$$

The calculated values of the above three parameters for precursor glass and glass ceramics are listed in Table 1.

Table 1
Radiative transition probabilities (A_{rad}), fluorescence branching ratios (β) and radiative decay time (τ_{rad}) of Er^{3+} in precursor glass and glass ceramics

Transition	$[U^2]^2$	$[U^4]^2$	$[U^6]^2$	G			600 GC			630 GC			630 GC			650 GC		
				A_{rad} (s^{-1})	β (%)	τ_{rad} (ms)	A_{rad} (s^{-1})	β (%)	τ_{rad} (ms)	A_{rad} (s^{-1})	β (%)	τ_{rad} (ms)	A_{rad} (s^{-1})	β (%)	τ_{rad} (ms)	A_{rad} (s^{-1})	β (%)	A_{rad} (ms)
$^4I_{13/2}\rightarrow{}^4I_{15/2}$	0.0195	0.1173	1.4316	120.2	100	8.32	119.8	100	8.30	121.7	100	8.22	119.9	100	8.34	121.8	100	8.21
$^4I_{11/2}\rightarrow{}^4I_{15/2}$	0.0282	0.0003	0.3953	114.5	80.7	7.10	103	80	7.8	110.3	80.5	7.30	110.8	80.6	7.30	110.2	80.4	7.30
$\rightarrow{}^4I_{13/2}$	0.0331	0.1708	1.0864	27.3	19.3		25.8	20		26.8	19.5		26.9	19.4		26.8	19.6	
$^4I_{9/2}\rightarrow{}^4I_{15/2}$	0	0.1732	0.0099	127.7	74.9	5.90	105.3	72.4	6.90	104.2	70.5	6.80	101.1	69.2	6.90	100.9	68.9	6.80
$\rightarrow{}^4I_{13/2}$	0.0004	0.0106	0.7162	39.5	23.2		37	25.4		40.4	27.3		41.6	28.5		42.1	28.8	
$\rightarrow{}^4I_{11/2}$	0.0030	0.0674	0.1271	3.3	1.9		3.2	2.2		3.2	2.2		3.3	2.3		3.4	2.3	
$^4F_{9/2}\rightarrow{}^4I_{15/2}$	0	0.5354	0.4619	1124.3	90.8	0.81	972.8	90.8	0.93	1001	90.7	0.91	996.2	90.7	0.91	996.0	90.7	0.91
$\rightarrow{}^4I_{13/2}$	0.0101	0.1533	0.0714	57.1	4.6		47.9	4.5		48.3	4.4		47.1	4.3		47.6	4.3	
$\rightarrow{}^4I_{11/2}$	0.0704	0.0112	1.2839	53.4	4.3		48.4	4.5		52	4.7		52.5	4.8		52.2	4.8	
$\rightarrow{}^4I_{9/2}$	0.1279	0.0059	0.0281	3.1	0.3		2.4	0.2		2.3	0.2		2.1	0.2		2.2	0.2	
$^4S_{3/2}\rightarrow{}^4I_{15/2}$	0	0	0.2211	891.6	66.0	0.74	838.4	66.1	0.79	916.2	66.2	0.72	945.6	66.3	0.70	940.1	66.2	0.70
$\rightarrow{}^4I_{13/2}$	0	0	0.3462	378.2	28.0		355.7	28.1		388.7	28.1		401.1	28.1		399.2	28.0	
$\rightarrow{}^4I_{11/2}$	0	0.0042	0.0739	28.9	2.2		27	2.1		29.3	2.1		30.1	2.1		30.6	2.2	
$\rightarrow{}^4I_{9/2}$	0	0.0788	0.2542	50.8	3.8		45.9	3.7		48.8	3.6		49.5	3.5		51.1	3.6	
$\rightarrow{}^4F_{9/2}$	0	0.0003	0.0264	0.5	0		0.5	0		0.6	0		0.6	0		0	0	
$^2H_{11/2}\rightarrow{}^4I_{15/2}$	0.7125	0.4123	0.0925	5185.8	95.4	0.18	3993.3	95.2	0.24	3907	95.1	0.24	3479.7	94.9	0	27	3499.7	94.7
$\rightarrow{}^4I_{13/2}$	0.0230	0.0611	0.0529	98.8	1.8		81.2	2.0		81.9	2.0		77.8	2.1		76.5	2.1	
$\rightarrow{}^4I_{11/2}$	0.0357	0.1382	0.0371	57.1	1.1		46.1	1.1		45.8	1.1		43.1	1.2		47.3	1.3	
$\rightarrow{}^4I_{9/2}$	0.2077	0.0662	0.2858	75.7	1.4		60.8	1.4		61.2	1.5		56.6	1.5		61.3	1.7	
$\rightarrow{}^4F_{9/2}$	0.3629	0.0224	0.0022	17.6	0.3		13.3	0.3		13	0.3		11.3	0.3		11.0	0.2	
$\rightarrow{}^4S_{3/2}$	0	0.1988	0.0101	0	0		0	0		0	0		0	0		0	0	

3.3. Near-infrared fluorescence and decay

Owing to the important potential application of 1530 nm emission, the spectral features of the $^4I_{13/2} \rightarrow {}^4I_{15/2}$ transition of Er^{3+} ions was specifically examined. The emission spectra, recorded under the same instrumental conditions, of this transition for all the samples with the same thickness are shown in Fig. 5. The relative intensity of the peak at 1546 nm and the integral intensity of 1530 nm emission (as shown in Fig. 6) increase obviously with the increasing of heating temperature, implying the alteration of Er^{3+} environment, in other words, more CaF_2 nano-crystals containing Er^{3+} were precipitated among the glass matrix. For precursor glass, the visible up-conversion emission was too weak to detect when pumped at 980 nm, while for glass ceramic the green ($^2H_{11/2}$, $^4S_{3/2} \rightarrow {}^4I_{15/2}$) and red ($^4F_{9/2} \rightarrow {}^4I_{15/2}$) emissions were recorded under the same conditions, as presented in the inset of Fig 6. With increasing of heating temperature, the intensities of visible up-conversion emissions were monotonously enhanced, as shown in Fig. 6, further revealing Er^{3+} ions entered into CaF_2 nano-crystals. The low phonon energy circumstance of CaF_2 nano-crystals (about 280 cm^{-1} [27]) is beneficial to the efficient up-conversion emissions of Er^{3+} [28]. For EDFA application, the up-conversion emission is a disadvantage to the 1.53 μm emission. To enhance the 1.53 μm emission intensity, it is helpful to introduce trivalent cerium ions to Er^{3+}-doped hosts [29,30]. Indeed, it was reported that the addition of Ce^{3+} ions enabled increase of laser slope efficiency by a factor of 2 and decrease of laser threshold to about 20% for Er^{3+}-doped $Ca_2Al_2SiO_7$ crystal [31], due to the reduction of up-conversion losses. In addition, recent investigation indicates that the introducing of Ce^{3+} to the glass ceramic containing PbF_2 nano-crystals depressed Er^{3+} up-conversion emission, and, as a consequence, enhanced 1.53 μm fluorescence [32]. Therefore, in order to further improve the near-infrared emission of our system, Er^{3+}/Ce^{3+} co-doping seems to be a desirable route.

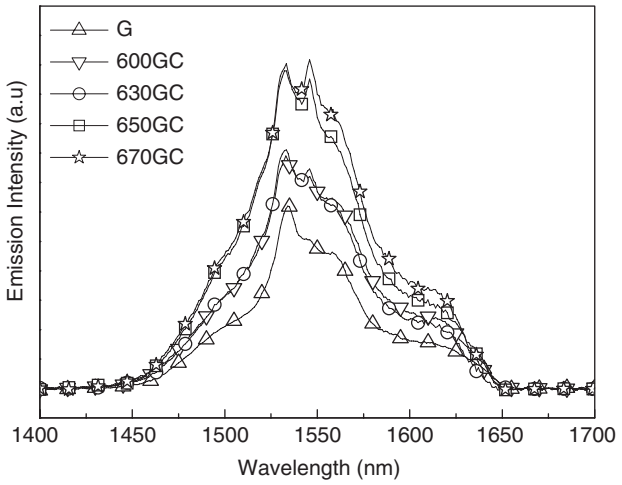

Fig. 5. Room temperature emission spectra of the $^4I_{13/2} \rightarrow {}^4I_{15/2}$ transition of Er^{3+} in precursor glass and glass ceramics.

The emission peak wavelength λ_e and the full width at half maximum (FWHM) of these spectra are listed in Table 2. The FWHM of glass ceramics is slightly larger than that of precursor glass. The FWHM of the emission band of Er^{3+} at 1.53 μm is an important parameter for EDFA. It is commonly expected that the emission band will be narrower in glass ceramics than in the corresponding precursor glass due to the lack of the disorder inhomogeneous broadening, as had indeed been observed in some Er^{3+}-doped glass ceramics [33,34]. However, the

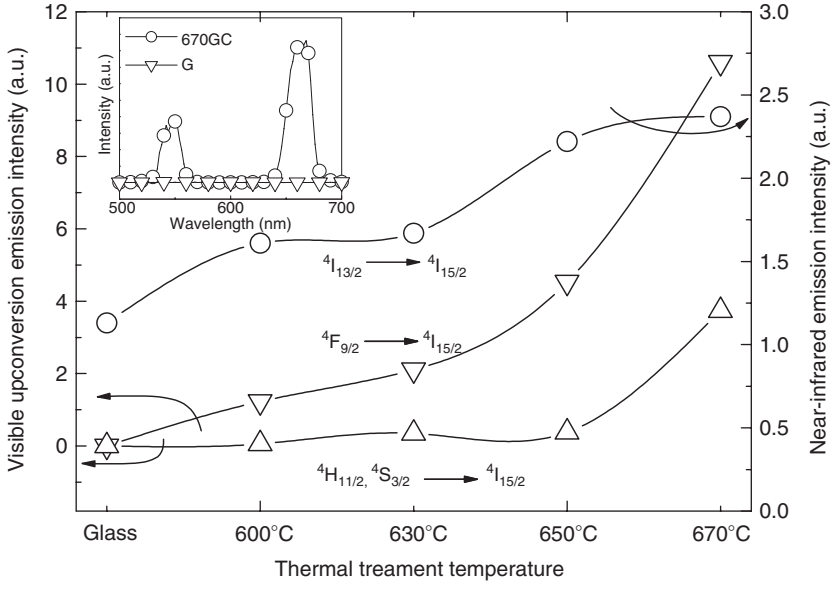

Fig. 6. Variation of near-infrared and visible up-conversion emission intensities of Er^{3+} versus thermal treatment temperature; the inset shows the up-conversion fluorescence spectra at room temperature.

Table 2
Judd–Ofelt intensity parameters and spectroscopic parameters for the $^4I_{13/2} \rightarrow {}^4I_{15/2}$ transition of Er^{3+} ions in precursor glass and glass ceramics

Sample	Ω_2 (10^{-20} cm^2)	Ω_4 (10^{-20} cm^2)	Ω_6 (10^{-20} cm^2)	τ_{rad} (ms)	τ_{exp} (ms)	η(%)	λ_e (nm)	FWHM (nm)	$\sigma_{em}(\lambda_e)$ (10^{-20} cm^2)
G	4.40	1.61	1.12	8.32	5.84	70.3	1534	73	0.52
600 GC	3.31	1.32	1.06	8.30	6.20	74.7	1533	85	0.45
630 GC	3.22	1.30	1.15	8.22	6.85	83.3	1533	80	0.48
650 GC	2.79	1.25	1.19	8.34	7.12	85.4	1533	81	0.47
670 GC	2.70	1.14	1.27	8.21	8.03	97.8	1546	85	0.45

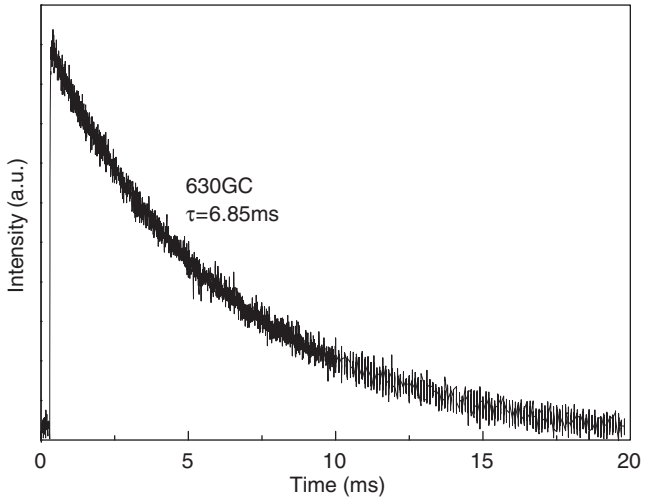

Fig. 7. A typical decay curve of 1530 nm emission in glass ceramic obtained by heat treated at 630 °C.

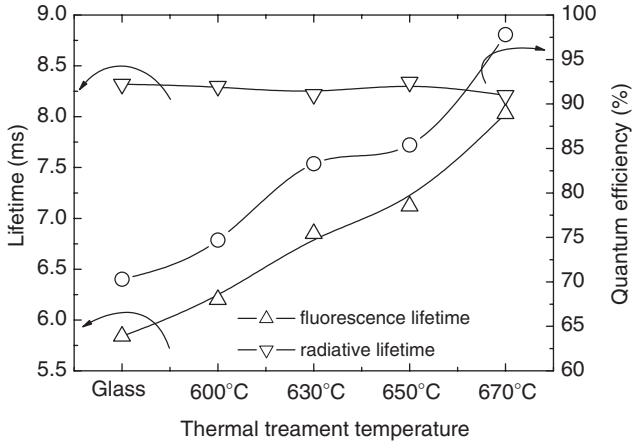

Fig. 8. Variation of fluorescence and radiative lifetime and quantum efficiency of Er^{3+} versus thermal treatment temperature.

FWHM of Er^{3+} in glass ceramics at 1.53 μm emission is larger than that of corresponding glass in our system. Rodriguez et al. had reported the similar phenomenon for glass ceramics containing PbF_2 nano-crystals and ascribed it to the thermal population of higher Stark sublevels in the excited $^4I_{13/2}$ state by investigating the low-temperature behaviors of absorption and emission spectra of Er^{3+} [35]. This mechanism could also be applicable to explain our result. In addition, the complementary emissions of Er^{3+} in CaF_2 and the residual Er^{3+} in glass matrix may also contribute to the broadening of FWHM.

A typical decay curve of $^4I_{13/2} \rightarrow {}^4I_{15/2}$ transition for 630 GC sample is shown in Fig. 7. Because of the non-exponential nature the effective decay time was calculated by

$$\tau_{exp} = \int I(t)\,dt/I_p, \tag{4}$$

where I_p is the peak intensity in the decay curve. With these measured values quantum efficiency (η) was calculated as the ratio of the effective fluorescence decay time to the radiative decay time ($\tau_.$) and the results are presented in Fig. 8. It can be seen that the radiative quantum efficiency obviously increases with the increasing of heating temperature due to the incorporation of more Er^{3+} into CaF_2 with lower phonon energy that reduces non-radiative relaxation. The stimulated emission cross sections of the $^4I_{13/2} \rightarrow {}^4I_{15/2}$ transition could be estimated from the emission spectra by [36]

$$\sigma_{em}(\lambda) = \frac{\lambda^5 \beta I(\lambda)}{8\pi c n^2 \int \lambda I(\lambda)\,d\lambda} \sum A_{JJ'}, \tag{5}$$

where $I(\lambda)$ is the emission intensity at wavelength λ. The exact values of $\sigma_{em}(\lambda_e)$, τ_{rad}, τ_{exp} and η are also summarized in Table 2.

Table 3
Comparison of the spectroscopic parameters of Er^{3+} in different host materials

Host materials	λ_e (nm)	FWHM (nm)	σ_e (10^{-20} cm^2)	η (%)	Ref.
670 GC	1546	85	0.45	98	This work
ZBLAN	1550	82	0.42	91	[37]
ED-2 (silicate)	—	40	0.65	100	[38]

At present, the silica-based and ZBLAN glasses are widely used as the media of the EDFA. As listed in Table 3, the FWHM values of the silica-based and ZBLAN glasses are about 40 and 80 nm, respectively. It is evident that the FWHM of 670 GC about 85 nm is wider than that of the silica-based glass and comparable to that of the ZBLAN glass. In addition, a large stimulated emission cross-section and high radiative quantum efficiency benefit the high gain and low threshold in laser operation. These two values for 670 GC are close to those of silica-based glass and ZBLAN.

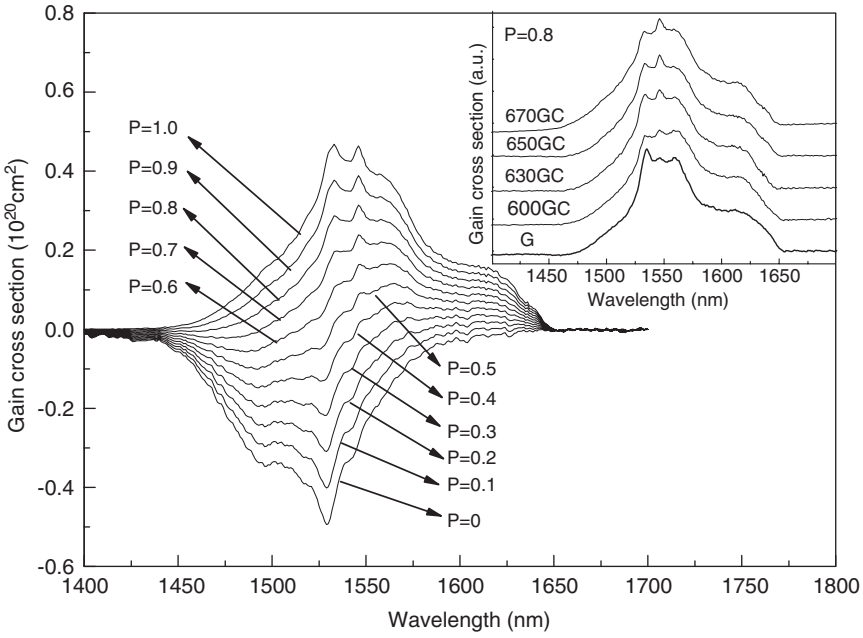

Fig. 9. Gain cross-section spectra of the $^4I_{13/2} \rightarrow {}^4I_{15/2}$ transition of Er^{3+} at different population inversion P for 650 GC sample; the inset shows the gain cross-section spectra for all samples at $P = 0.8$.

3.4. 1.53 μm emission gain cross-section spectra

For laser application, one of the relevant parameters is the gain cross-section, which is calculated by

$$g(\lambda) = P\sigma_{em}(\lambda) - (1 - P)\sigma_{abs}(\lambda), \quad (6)$$

where the population inversion P is the ratio of Er^{3+} concentration in the excited state $^4I_{13/2}$ over that in the ground state, and σ_{abs} the absorption cross-section. All the samples exhibit relatively flat gain cross-section for the population inversion ranging from 0.7 to 1.0. As an example, Fig. 9 displays the gain cross-section spectra for P ranging from 0 to 1. The curves of absorption and emission cross-section are presented for $P = 0$ and 1, respectively. The inset of Fig. 9 shows gain cross-section for all the samples at $P = 0.8$. Obviously, the gain spectra in the range from 1530 to 1565 nm are relatively flat, which covers the C-band of telecommunication, indicating the potential applicability of the investigated oxyfluoride glass and glass ceramics as EDFA.

4. Conclusions

Spectroscopic measurements and analysis based on Judd–Ofelt theory on Er^{3+}-doped glass ceramic nanocomposites thermal treated at different temperatures demonstrated that, with increasing of heating temperature, the emission lifetime, the quantum efficiency and the intensities of near-infrared and up-conversion emissions increased significantly, attributing to the fact that more fraction of Er^{3+} ions incorporated into the precipitated CaF_2 nano-crystals with lower phonon energy. Broad bandwidth and large stimulated emission cross-section of 1.53 μm fluorescence were obtained, and the gain cross-sections were computed to be relatively flat in the range from 1530 to 1565 nm for population inversion from 0.7 to 1.0 for the investigated systems.

Acknowledgments

This work was supported by the project of Nano-molecular Functional Materials of Fujian Province (2005HZ01-1), the grant of the Natural Science Foundation of Fujian Province (A0320001) and the State Key Laboratory of Structural Chemistry of China (050005).

References

[1] B.D. Bartolo, Radiationless Processes, Plenum, New York, 1980.
[2] M. Mortier, F. Auzel, J. Non-Cryst. Solids 256–257 (1999) 361.
[3] A. Lucca, M. Jacquemet, F. Druon, F. Balembois, P. Georges, P. Camy, J.L. Doualan, R. Moncorgé, Opt. Lett. 29 (2004) 1879.
[4] Y. Wang, J. Ohwaki, Appl. Phys. Lett. 63 (1993) 3268.
[5] V.K. Tikhomirov, D. Furniss, A.B. Seddon, I.M. Reaney, M. Beggiora, M. Ferrari, M. Montagna, R. Rolli, Appl. Phys. Lett. 81 (2002) 1937.
[6] J. Mendéz-Ramos, V.K. Tikhomirov, A.B. Seddon, V.D. Rodríguez, Phys. Stat. Sol. A 201 (2004) R57.
[7] D.Q. Chen, Y.S. Wang, Y.L. Yu, Z.J. Hu, Mater. Sci. Eng. B 123 (2005) 1.
[8] B.R. Judd, Phys. Rev. 127 (1962) 750.
[9] G.S. Ofelt, J. Chem. Phys. 37 (1962) 511.
[10] J. Méndez-Ramos, V. Lavín, I.R. Martín, U.R. Rodríguez-Mendoza, J.A. González-Almeida, V.D. Rodríguez, A.D. Lozano-Gorrín, P. Núñez, J. Alloys Comp. 323–324 (2001) 753.
[11] M. Abril, J. Méndez-Ramos, I.R. Martín, U.R. Rodríguez-Mendoza, V. Lavín, P. Núñez, A.D. Lozano-Gorrín, J. Appl. Phys. 95 (2004) 5271.

[12] X. Qiao, X. Fan, M. Wang, X. Zhang, Opt. Mater. 27 (2004) 597.
[13] X. Qiao, X. Fan, J. Wang, M. Wang, J. Non-Cryst. Solids 351 (2005) 357.
[14] D.Q. Chen, Y.S. Wang, Y.L. Yu, E. Ma, Z.J. Hu, J. Phys: Condens. Matter 17 (2005) 6545.
[15] F. Lahoz, I.R. Martín, U.R. Rodríguez-Mendoza, I. Iparraguirre, J. Azkargorta, A. Mendioroz, R. Balda, J. Fernández, V. Lavín, Opt. Mater. 27 (2005) 1762.
[16] A.G. Souza Filho, J. Mendes Filho, F.E.A. Melo, M.C.C. Custódio, R. Lebullenger, A.C. Hernandes, J. Phys. Chem. Solids 61 (2000) 1535.
[17] R.T. Génova, I.R. Martín, U.R. Rodríguez-Mendoza, F. Lahoz, A.D. Lozano-Gorrín, P. Núñez, J. González-Platas, V. Lavín, J. Alloys Comp. 380 (2004) 167.
[18] H. Sun, L. Zhang, M. Liao, G. Zhou, C. Yu, J. Zhang, L. Hu, Z. Jiang, J. Lumin. 117 (2006) 179.
[19] P.A. Tick, Opt. Lett. 23 (1998) 1904.
[20] C.K. Jorgensen, B.R. Judd, Mol. Phys. 8 (1964) 281.
[21] X. Zou, T. Izumitani, J. Non-Cryst. Solids 162 (1993) 68.
[22] M. Bettinelli, A. Speghini, M. Ferrari, M. Montagna, J. Non-Cryst. Solids 201 (1996) 211.
[23] E.W.J.L. Oomen, A.M.A. van Dongen, J. Non-Cryst. Solids 111 (1989) 205.
[24] Y. Nageno, H. Takebe, K. Morinaga, T. Izumitani, J. Non-Cryst. Solids 169 (1994) 288.
[25] S. Tanabe, T. Ohyagi, N. Soga, T. Hanada, Phys. Rev. B 46 (1992) 3305.
[26] W.T. Carnal, I.P.R. Fields, K. Rajnak, J. Chem. Phys. 49 (1968) 4424.
[27] G.A. Kumar, R. Riman, S.C. Chae, Y.N. Jang, I.K. Bae, H.S. Moon, J. Appl. Phys. 95 (2004) 3243.
[28] D.Q. Chen, Y.S. Wang, Y.L. Yu, E. Ma, F. Bao, Z.J. Hu, Y. Cheng, Mater. Chem. Phys. 95 (2006) 264.
[29] B. Simondi-Tessaire, B. Viana, D. Vivien, A.M. Lejus, Opt. Mater. 6 (1996) 267.
[30] J. Yang, L. Zhang, L. Wen, S. Dai, L. Hu, Z. Jiang, Chem. Phys. Lett. 384 (2004) 295.
[31] B. Simondi-Tessaire, B. Viana, A.M. Lejus, J.M. Benitez, D. Vivien, C. Borel, R. Templier, C. Wyon, IEEE J. Quant. Electron. 32 (1996) 2004.
[32] G. Dantelle, M. Mortier, D. Vivien, G. Patriarche, Chem. Mater. 17 (2005) 2216.
[33] M. Mortier, P. Goldner, C. Chateau, M. Genotelle, J. Alloys Comp. 323–324 (2001) 245.
[34] M. Mortier, A. Montevillie, G. Patriarche, G. Maze, F. Auzel, Opt. Mater. 16 (2001) 255.
[35] V.D. Rodríguez, V.K. Tikhomirov, J. Mendéz-Ramos, A.B. Seddon, Europhys. Lett. 69 (2005) 128.
[36] A.A. Kaminskii, Laser Crystals, Their Physics and Properties, Springer, New York, 1989.
[37] L. Wetenkamp, G.F. West, H. Tobben, J. Non-Cryst. Solids 140 (1992) 35.
[38] V.P. Gapontsev, S.M. Matitsin, A.A. Isineev, V.B. Kravchenko, Opt. Laser Technol. 14 (1982) 189.